Structures of surfaces and amorphous samples obtained by EXAFS measurements in the x-ray Raman-scattering mode

Faris Gel'mukhanov*
Institute of Physics, University of Uppsala, S-75121 Uppsala, Sweden

Hans Ågren
Institute of Physics and Measurement Technology, University of Linköping, S-58183, Linköping, Sweden
(Received 4 March 1994)

We present a theory for extended x-ray-absorption fine structures (EXAFS) measured in the x-ray Raman-scattering mode. Spectra of such structures can be obtained by scanning the frequency of the exciting x-ray photons over the EXAFS region while fixing the detector frequency to an emission resonance. It is shown that these spectra in addition to the structure-determining features of ordinary EXAFS allow us to obtain orientational information, that is, to obtain data on both bond lengths and on orientations of bonds. We derive the explicit dependence of spectral features on the angles between the bond direction and the dipole moment direction of an x-ray-emission transition. Since each resonance frequency is associated with a specific direction of the transition dipole, rich possibilities prevail for orientational information within a molecular framework. We show that measurements of extended x-ray-absorption fine structures in the x-ray Raman-scattering mode also allow us to obtain bond angles of disordered systems such as glasses or free molecules, for which conventional x-ray-diffraction methods do not apply. A comparative discussion is given on the prospects of EXAFS experiments in the nonradiative (Auger) scattering mode.

I. INTRODUCTION

X-ray-absorption cross sections can show oscillatory structures extending far beyond the ionization edge. The physical mechanism behind these oscillations, commonly denoted as EXAFS (x-ray-absorption fine structure), is given by the interference between the outgoing photoelectron wave from the adsorbing atom and the backscattered waves from the surrounding atoms.[1] A remarkable increase in attention to EXAFS took place after the publication of the papers of Sayers, Lytle, and Stern,[2,3] which showed that techniques based on EXAFS can actually yield structure information on complex molecular or condensed systems even in cases when other traditional structure methods, such as x-ray diffraction, are not applicable.

EXAFS analysis of disordered systems can give information on the distances $R_{\alpha\alpha_1}$ between the absorbing atom α and the neighboring high-Z atoms α_1.[1-4] The angle between the polarization vector $\mathbf{e}$ of the absorbed x-ray photons and the internuclear axis direction $\mathbf{R}_{\alpha\alpha_1}$ can be measured only when the EXAFS technique is applied to well-ordered systems like crystals, surfaces, and adsorbates on single-crystal surfaces.[1,4-6] In the last case, measurements of surface extended x-ray-absorption fine structure (SEXAFS) (Refs. 1, 5, and 6) make it possible to determine the internuclear distances $R_{\alpha\alpha_1}$ and the chemisorption sites. At the present time several modifications of the E XAFS technique are utilized.[1,4] These are ordinary EXAFS measured in the direct transmission mode, EXAFS obtained by a partial-electron-yield detection mode,[1,4] and EXAFS obtained by the partial-fluorescence-yield (FY) mode.[1,4-6] In some cases it is possible to detect EXAFS only in the fluorescence-yield mode because of the smaller penetration depth of electrons with respect to photons.[5] The corresponding measurements became possible with the advent of high-intensity x-ray sources derived from synchrotron radiation. The utility of EXAFS detected in the FY mode is based on the assumption of proportionality between the x-ray fluorescence yield and the x-ray-absorption cross section $\sigma^{XA}(\omega)$ for samples of small thickness.[1,4] Assuming this model, the absorption cross section is obtained by detecting the emission of x-ray photons associated with the secondary process of core-hole annihilation. However, the limitations of such a two-step model for the x-ray fluorescence process were early realized,[7-11] and a unified picture of x-ray fluorescence as a process of inelastic x-ray scattering (IXS) or x-ray Raman scattering (XRS) was called for. As demonstrated here, the use of inelastic x-ray scattering gives qualitatively different and much richer information on the geometrical structure of condensed or molecular systems.

The oscillatory part of the x-ray-absorption cross section $\sigma^{XA}(\omega)$ in the EXAFS region is proportional to $(\mathbf{e}\cdot\mathbf{R}_{\alpha\alpha_1})^2$ for well-ordered samples, like crystals or metallic surfaces.[1,4] This fact makes it possible to determine, for example, the chemisorption site of an adsorbed molecule at a surface,[1,5,6] but it is still difficult to define the orientation of adsorbed molecules relative to the surface by this method (however, see Ref. 12). Moreover, traditional EXAFS does not give directional information, like angles between internuclear axes, for noncrystalline sys-

tems such as amorphous semiconductors, liquids, or free molecules. This situation changes qualitatively when the x-ray-absorption spectrum is measured in the XRS (or IXS) mode, which is the main message of the present article. The measured fluorescent signal will be proportional to

$$(\mathbf{e}'\cdot\mathbf{d}_n)^2\sigma^{\mathrm{XA}}(\omega) \tag{1}$$

and as a result it will depend on the mutual orientation of the polarization vector $\mathbf{e}'$ of the emitted x-ray photon and the dipole moment $\mathbf{d}_n$ of the emissive transition from an occupied molecular orbital $|n\rangle$. Taking into account that the direction of the dipole moment $\mathbf{d}_n$ is connected directly with the space orientation of the molecular axis, and that the oscillatory part of the XRS cross section is proportional to $(\mathbf{e}'\cdot\mathbf{d}_n)^2(\mathbf{e}\cdot\mathbf{R}_{\alpha\alpha_1})^2$, one can understand that the detection of EXAFS in the XRS mode can give directional information as well as information on internuclear distances. At first sight one cannot receive information about molecular structure or bond angles of disordered systems using the XRS method due to averaging of the scattering cross section over molecular orientations (we shall use the term "molecule" for the nearest surroundings of an adsorbing atom). However, this is not the case after a closer inspection; the oscillatory part of the XRS cross section averaged over molecular orientations must depend on the $\mathbf{e}$, $\mathbf{e}'$, $\mathbf{d}_n$, and $\mathbf{R}_{\alpha\alpha_1}$ vectors only through the two scalar products $(\mathbf{e}\cdot\mathbf{e}')$ and $(\mathbf{d}_n\cdot\mathbf{R}_{\alpha\alpha_1})$ of external and internal vectors, respectively. As a result, the XRS cross section cannot be given as a simple product of emission and absorption probabilities. Moreover, this circumstance causes a strong dependence of the EXAFS spectral shape on polarization directions $\mathbf{e}$ and $\mathbf{e}'$ and on the frequency of the emitted x-ray photon. In the case of near-edge EXAFS (NEXAFS) we investigated a related effect recently.[11] As shown in this article the dependence of EXAFS detected in the XRS mode on the scalar product $(\mathbf{d}_n\cdot\mathbf{R}_{\alpha\alpha_1})$ gives the possibility of measuring bond angles of disordered systems. The effect considered here is connected with the small anisotropy of x-ray fluorescence under excitation of core electrons to the far continuum. It was shown early[10,13,14] that the anisotropy of x-ray fluorescence of disordered systems is large when the frequency of the incoming x-ray photons is near the absorption threshold but small if this frequency is far from the threshold. We will show that this small anisotropy still plays a principal role and that it gives quantitatively strong effects when the XRS process is used for EXAFS measurements.

The paper is organized as follows. A general theory of EXAFS measured in the XRS mode is given in Sec. II. Section III presents the main polarization properties of EXAFS of ordered and disordered systems. In Sec. IV we illustrate some useful aspects of the general theory by means of an application to amorphous silicon oxide. Our findings are discussed and concluded in the last sections, Secs. V and VI. In Sec. V we also discuss the prospects of EXAFS measured in the nonradiative Auger mode.

II. INELASTIC SCATTERING OF X-RAY PHOTONS ABOVE IONIZATION THRESHOLD

Resonant inelastic x-ray scattering is a two-photon process, the double-differential cross section of which in the weak-photon field limit is described by the Kramers-Heisenberg formula[7-10,15]

$$\frac{d^2\sigma}{d\omega' d\Omega}=\sum_{\nu}\sum_{n}\frac{\omega'}{\omega}|F_{\nu n}(\omega)|^2\Delta(\omega-\omega'-\omega_{\nu n},\Gamma_{\nu n})\ , \tag{2}$$

which takes into account the final-state lifetime broadening $\Gamma_{\nu n}$. Here

$$\Delta(\omega,\Gamma)=\frac{\Gamma}{\pi(\omega^2+\Gamma^2)}\ , \tag{3}$$

$\omega_{\nu n}$ is the resonant frequency of the optical transition $n\rightarrow\nu$, and $d\Omega$ is the solid angle of photon scattering. The partial or channel amplitude $F_{\nu n}(\omega)$ of x-ray scattering,

$$F_{\nu n}(\omega)=\alpha\omega_\nu\omega_n(\nu)\frac{(\mathbf{e}^*\cdot\mathbf{d}_\nu)[\mathbf{e}'\cdot\mathbf{d}_n(\nu)]}{\omega-\omega_\nu+i\Gamma_\nu}\ , \tag{4}$$

describes the two-photon process of absorption of incoming and emission of final x-ray photons, the frequencies and polarization vectors of which are ω,ω' and $\mathbf{e},\mathbf{e}'$, respectively. We use atomic units ($\hbar=m=e=1$, $\alpha=\frac{1}{137}$) and the following notation: $\omega_\nu=E(c^{-1}\nu)-E_0$, $\omega_n(\nu)=E(c^{-1}\nu)-E(n^{-1}\nu)$, $\mathbf{d}_\nu=\langle 0|\mathbf{d}|c^{-1}\nu\rangle$, and $\mathbf{d}_n(\nu)=\langle c^{-1}\nu|\mathbf{d}|n^{-1}\nu\rangle$ for the resonant frequencies and dipole matrix elements of x-ray absorption ($c\rightarrow\nu$) and emission ($n\rightarrow c$) transitions, respectively; $\omega_{\nu n}=E(n^{-1}\nu)-E_0$ is a frequency for the optical excitation $n\rightarrow\nu$ and is equal to the difference between energies $E(n^{-1}\nu)$ and E_0 of excited $|n^{-1}\nu\rangle$ and ground $|0\rangle$ molecular states; and Γ_ν is the half width at half maximum (HWHM) of the x-ray absorption line $c\rightarrow\nu$. The electron excited to the vacant molecular orbital (MO) ψ_ν screens differently the subsequent decay of electrons from various occupied levels n to the inner shell c. This specific screening effect leads to a dependence on ν of the frequencies $\omega_n(\nu)$ and the dipole matrix elements $\mathbf{d}_n(\nu)$. In formula (4) we have ignored the small normal and anomalous nonresonant terms. The normal nonresonant term is only important far from resonance, for example, in the cases of Rayleigh or Thomson scattering. The nonresonant anomalous scattering term is generally believed to give only minor contributions to the XRS process, and at resonance the contribution from this term is negligible; see, for example, the discussion by Sakurai.[15] The ratio of nonresonant to resonant amplitudes (4) is of the order of $r_0/\lambda\ll 1$.[10] Here $r_0\simeq 2.8\times10^{-13}$ cm is the classical radius of the electron and $\lambda\sim10^{-6}$–10^{-7} cm is the wavelength of the x-ray photon.

As mentioned above, fluorescence-yield measurements of x-ray absorption spectra can be carried out by tuning the frequency ω' to an exact resonance of some emission transition $n\rightarrow c(\omega'=\omega_{n(\nu)})$ between an occupied MO n and a core hole c. In such a case one can neglect nonresonant terms in Eq. (2), implying the following function

for the resonant value: $\sigma_n(\omega)=d^2\sigma/d\omega' d\Omega$. The lifetime broadening of optical transitions is negligibly small in comparison with the width of x-ray transitions. This allows us to assume that $\Gamma_{vn}=0$ and to replace the Δ function (3) by the Dirac δ function $\delta(\omega-\omega'-\omega_{vn})$ in Eq. (2). As a result the resonant value of the cross section (2) can be written in a one-electron approximation as

$$\sigma(\omega)=q(\mathbf{e}'\cdot\hat{\mathbf{d}}_n)^2\sum_c\sum_v\langle c|\mathbf{e}\cdot\mathbf{r}|v\rangle\delta(E-E_v)\langle v|\mathbf{e}\cdot\mathbf{r}|c\rangle\ . \tag{5}$$

Here $E=\omega-I$ is the detuning of the absorbed x-ray photon frequency ω relative to the ionization potential (I) of a core electron in the state $|c\rangle$ and $E_v=\omega_v-I$ is the one-electron energy of an unoccupied MO $|v\rangle$ or the energy of the photoelectron measured relative to the absorption edge when $\omega>I$; $\mathbf{r}$ is a radius vector of the electron; $q=\alpha^2 d^2_{n(v)}\omega^2_v\omega^3_{n(v)}/(\omega\Gamma^2_v)$; and $\hat{\mathbf{d}}=\mathbf{d}/d$ is a unit vector directed along $\mathbf{d}$. To evaluate the cross section (5) we require the matrix elements of the imaginary part of the one-particle Green function's operator

$$\mathrm{Im}G^+_E=-\pi\sum_v|v\rangle\delta(E-E_v)\langle v|\ . \tag{6}$$

The operator $G^+_E=(E-H+i\epsilon)^{-1}$, expressed through the corresponding one-electron Hamiltonian (H), defines the relevant Green's function $G^+_E(\mathbf{r},\mathbf{r}')$ to be that for the outward propagating wave ($\epsilon\rightarrow+0$). The formula for the resonance value of the cross section (5) now becomes

$$\sigma(\omega)=-\frac{q}{\pi}(\mathbf{e}'\cdot\mathbf{d}_n)^2\sum_c\mathrm{Im}\langle c|\mathbf{e}\cdot\mathbf{r}G^+_E\mathbf{e}\cdot\mathbf{r}|c\rangle\ . \tag{7}$$

Let us consider inelastic scattering of x-ray photons with frequency ω above the ionization threshold for core-electron ionization. To investigate this problem analytically we need to make some additional assumptions. A well-known model that leads to analytical solutions of this problem is the muffin-tin (MT) or Korringa-Kohn-Rostoker (KKR) approximation.[1] In this approximation the potential experienced by the final-state photoelectron is represented by a system of nonoverlapping spherically symmetric potentials, centered around each atomic site $\mathbf{R}_\alpha$. The potential between the muffin tins is constant. The main conclusions in the present work are not dependent on the MT approximation as such, but, apart from allowing analytical derivations, the MT approximation is numerically excellent for high-energy excitations in the EXAFS region. In this case the scattering of high-energy photoelectrons by atom α takes place within a subatomic characteristic region with the size of $\sim k^{-1}$, clearly "within" atom α. For low-energy photoelectrons in the NEXAFS "shape-resonant" region it is well known that a full account of the molecular potential gives better results.

The main properties of the Green's function $G^+_E(\mathbf{r},\mathbf{r}')$ (Refs. 16–18) in the MT approximation are collected in the Appendix. We use the index α to denote the central atom, the core electron of which is excited into the continuum under inelastic x-ray scattering. The expansion of the Green's function over spherical functions $Y_{lm}(\hat{\boldsymbol{\rho}})$ inside this αth MT sphere [see Eq. (A1) of the Appendix] leads to the following formula for the K cross section of inelastic x-ray scattering given by (7):

$$\sigma(\omega)=3\sigma_0(\omega)(\mathbf{e}'\cdot\hat{\mathbf{d}}_n)^2(1+\chi)\ . \tag{8}$$

The deviation of this cross section from the scattering cross section by the isolated atoms is described by the χ function:

$$\chi=-\mathrm{Im}\sum_{mm'}e^{2i\delta^\alpha_1}(\mathbf{e}_m G^{\alpha\alpha'}_{1m1m'}\mathbf{e}_{m'})\ , \tag{9}$$

where δ^α_1 is the p phase shift in the potential for the absorbing atom α. We have for simplicity here assumed x-ray scattering of K electrons; corresponding formulas for L, M, . . . x-ray scattering can be obtained straightforwardly. The total inelastic scattering cross section $4\pi\sigma_0(\omega)=\frac{8}{9}kqP^2$ by the isolated atom α is proportional to the wave number $k=(2E)^{1/2}$ of the photoelectron and to the square of the dipole momentum integral

$$P=\int_0^{a_\alpha}d\rho\,\rho^3R^\alpha_0(\rho)R^\alpha_1(\rho)\ . \tag{10}$$

Here $R^\alpha_0(\rho)$ is the radial part of the K-electron wave function while $R^\alpha_1(\rho)$ is the regular radial part of the photoelectron wave function with $l=1$ (see the Appendix); a_α is the radius of the αth sphere. One can see that the right-hand side of Eq. (8) contains the x-ray-absorption cross section[1–4]

$$\sigma^{\mathrm{XA}}(\omega)=\sigma^{\mathrm{XA}}_0(\omega)(1+\chi)\ , \tag{11}$$

where $\sigma^{\mathrm{XA}}_0(\omega)$ is the x-ray-absorption cross section for the isolated atom α. The inelastic x-ray-scattering cross section (8) differs from the one of x-ray absorption (11) by the multiplier $(\mathbf{e}'\cdot\hat{\mathbf{d}}_n)^2$. As shown earlier,[13] this difference leads to important experimental consequences[14] when the frequency ω of the absorbing x-ray photon is close to the ionization threshold for the core electron. Here we will see that the term $(\mathbf{e}'\cdot\hat{\mathbf{d}}_n)^2$ can give information about the geometrical structure of the nearest surroundings of an absorbing atom α. The structure information is obtained from the x-ray-absorption measurements on the high-energy side of the x-ray-absorption edges where the oscillations of the x-ray-absorption cross section (EXAFS) take place. These oscillations are described by the χ function of Eq. (9).

Let us investigate the properties of inelastic x-ray scattering on the high-energy side of the x-ray-absorption edges. At sufficiently high energies the photoelectron wave length $\lambda=2\pi/k$ is smaller than the interatomic distance $R_{\alpha\alpha'}(\mathbf{R}_{\alpha\alpha'}=\mathbf{R}_\alpha-R_{\alpha'})$,

$$kR_{\alpha\alpha'}\gg1\ . \tag{12}$$

Under this condition the following asymptotic formula is valid for the free-electron Green's function defined by Eq. (A6) in the Appendix:

$$g^{\alpha\alpha'}_{LL'}\approx-(1-\delta_{\alpha\alpha'})\frac{4\pi e^{ikR_{\alpha\alpha'}}}{kR_{\alpha\alpha'}}i^{l-l'}Y^*_L(\hat{\mathbf{R}}_{\alpha\alpha'})Y_{L'}(\hat{\mathbf{R}}_{\alpha\alpha'})\ . \tag{13}$$

Here $\delta_{\alpha\alpha'}$ is the Kronecker delta symbol. This formula says that we have to search for the solution of Eq. (A4) of the Appendix for the total Green's function $G_{LL'}^{\alpha\alpha'}$ in the form

$$G_{LL'}^{\alpha\alpha'}=-\frac{4\pi}{k}i^{l-l'}\left[(1-\delta_{\alpha\alpha'})\frac{e^{ikR_{\alpha\alpha'}}}{R_{\alpha\alpha'}}Y_L^*(\hat{\mathbf{R}}_{\alpha\alpha'})Y_{L'}(\hat{\mathbf{R}}_{\alpha\alpha'})+\sum_{\alpha''}Y_L^*(\hat{\mathbf{R}}_{\alpha\alpha''})q_{\alpha\alpha''\alpha'}^{L'}\right] . \tag{14}$$

The quantity $q_{\alpha\alpha''\alpha'}^{L}$ is the wave coming from atom α' and impinging on atom α as the result of scattering by atom α''. It is obtained as a solution of the following equations:

$$q_{\alpha\alpha''\alpha'}^{L}=\frac{e^{ik(R_{\alpha\alpha''}+R_{\alpha''\alpha'})}}{R_{\alpha\alpha''}R_{\alpha''\alpha'}}f_{\alpha''}(\vartheta_{\alpha\alpha''\alpha'})Y_L(\hat{\mathbf{R}}_{\alpha''\alpha'})+\frac{e^{ikR_{\alpha\alpha''}}}{R_{\alpha\alpha''}}\sum_{\alpha_1}f_{\alpha''}(\vartheta_{\alpha\alpha''\alpha_1})q_{\alpha''\alpha_1\alpha'}^{L} , \tag{15}$$

where $\vartheta_{\alpha\alpha''\alpha'}$ is the scattering angle of the photoelectron propagated from atom α' to atom α via the scattering atom α''

$$\cos(\vartheta_{\alpha\alpha''\alpha'})=(\hat{\mathbf{R}}_{\alpha\alpha''}\cdot\hat{\mathbf{R}}_{\alpha''\alpha'}) .$$

This scattering angle has the character of a classical electron trajectory, a notion that holds in the short-wave limit of Eq. (12). The scattering amplitude $f_\alpha(\vartheta)$ at angle ϑ between initial $\mathbf{k}$ and final $\mathbf{k}'$ wave vectors of the photoelectron is defined in the usual way:

$$f_\alpha(\vartheta)=\frac{2\pi}{ik}\sum_L(e^{2i\delta_l^\alpha}-1)Y_L(\hat{\mathbf{k}})Y_L^*(\hat{\mathbf{k}}') . \tag{16}$$

The physical content associated with Eq. (15), which is one of the main results of this paper, needs some further comments. The wave $q_{\alpha\alpha''\alpha'}^{L}$ is formed by two types of waves scattered by atom α'' and impinging on atom α. The first type is the Lth harmonic plane wave from atom α' [the first term of the right-hand side of Eq. (15)] impinging on atom α'', and the second type is the $q_{\alpha''\alpha_1\alpha'}^{L}$ wave impinging on atom α'' from atom α' due to the scattering by atom α_1 [the second term of the right-hand side of Eq. (15)]. The high-energy multiple-scattering (HEMS) equations (15) are the short-wave asymptotes (12) of the exact multiple-scattering MT equations (A4) for Green's function $G_{LL'}^{\alpha\alpha'}$, and they overcome many of the difficulties of the exact equations. The order of the HEMS equations is defined only by the number of atoms N, while the exact order of the MT equations depends both on N and on the maximum value $l_{\max}\sim kR$ of l.[19,20] The advantages of the HEMS equations are apparent, because in the EXAFS region $l_{\max}$ increases as $R\sqrt{2E}$. Equation (15) can give a strict solution without using the multiple-scattering (MS) expansion. Strictly speaking, the corresponding MS row diverges due the large amplitude $f_\alpha(0)$ of forward scattering[4,23] (see below, however). On the high-energy side of the absorption edge, both the inelastic x-ray-scattering (8) and the absorption cross sections (11) exhibit the EXAFS oscillations related to the atoms immediately surrounding the absorbing atom. This can be seen directly from the asymptotic expression for the χ function of Eq. (9),

$$\chi=\frac{\sqrt{12\pi}}{k}\mathrm{Im}\sum_{\alpha_1}\sum_m e^{2i\delta_1^\alpha}(\mathbf{e}\cdot\mathbf{R}_{\alpha\alpha_1})q_{\alpha\alpha_1\alpha}^{1m}\mathbf{e}_m^* , \tag{17}$$

where the summation over surrounding atoms does not include terms with $R_{\alpha\alpha'}=0$. Solving Eq. (15) iteratively one can receive the following[4,16,17,19–21] multiple-scattering expansion for the χ function:

$$\chi=-3\,\mathrm{Im}\sum_{\alpha_1}\frac{\exp[i(2\delta_1^\alpha+kR_{\alpha\alpha_1})]}{kR_{\alpha\alpha_1}}\left[\Lambda_{\alpha\alpha_1\alpha}(\mathbf{e}\cdot\hat{\mathbf{R}}_{\alpha\alpha_1})^2-\cdots-\sum_{\alpha_2}\cdots\sum_{\alpha_3}\sum_{\alpha_4}\Lambda_{\alpha\alpha_1\alpha_2}\cdots\Lambda_{\alpha_3\alpha_4\alpha}(\mathbf{e}\cdot\hat{\mathbf{R}}_{\alpha\alpha_1})(\mathbf{e}\cdot\hat{\mathbf{R}}_{\alpha_4\alpha})-\cdots\right] . \tag{18}$$

The term

$$\Lambda_{\alpha\alpha_1\alpha_2}=f_{\alpha_1}(\vartheta_{\alpha\alpha_1\alpha_2})\frac{e^{ikR_{\alpha_1\alpha_2}}}{R_{\alpha_1\alpha_2}}(1-\delta_{\alpha_1\alpha_2}) \tag{19}$$

describes a wave impinging on atom α_2 as a result of elastic scattering of the photoelectron by atom α_1 when this electron is coming from atom α. As was shown by Lee and Pendry[22] (see also Refs. 4 and 19) the series (18) has a poor convergence behavior due to the large magnitude of the forward-scattering amplitude $f_\alpha(0)$ compared with the backscattering one, $f_\alpha(\pi)$, or $f_\alpha(\theta)$ for finite scattering angles θ. Indeed, the parameter $|\Lambda_{\alpha_1\alpha\alpha_2}|$ equal to $|f_\alpha(0)|/R_{\alpha\alpha_2}$ is larger than 1 for forward scattering.[4,16,19–22] The problem of summing the divergent MS series (18) is resolved by direct solution of the multiple-scattering equation, Eq. (15). The MT approximation and the asymptotic form of the spherical Hankel function $[h_l^+(x)\approx i^{-(l+1)}\exp(ix)/x]$ constitute the basis for the MS Eq. (15) and the MS expansion (18). The high-energy expansion (18) is known as the plane-wave approximation (PWA).[22,24] Rehr and co-workers[24,25] created a generalization of the PWA expansion named the curved-wave MS (CWMS) method with a larger range of validity.

At the present time the one-scattering approximation[1–4]

$$\chi=-3\,\mathrm{Im}\sum_{\alpha_1}\frac{\exp[2i(kR_{\alpha\alpha_1}+\delta_1^{\alpha})]}{kR_{\alpha\alpha_1}^2}f_{\alpha_1}(\pi)(\mathbf{e}\cdot\hat{\mathbf{R}}_{\alpha\alpha_1})^2 \quad (20)$$

has the broadest applications. A more convincing point of view on the problem of multiple scattering in the EXAFS theory was developed in the works presented in Refs. 20, 23, and 24. The results of some model investigations by Rehr and Stern and Schaich[20,23] show that summing the forward-scattering terms to all orders leads only to renormalized values for the wave number k and the phase shift δ_1^{α} in Eq. (20).

III. POLARIZATION PROPERTIES OF ORDINARY EXAFS AND EXAFS MEASURED IN THE RESONANT INELASTIC X-RAY SCATTERING MODE

Equations (8), (11), and (20) show that the polarization dependence of the EXAFS signal is qualitatively different when measured in the XRS mode than when measured by the ordinary x-ray-absorption method. While the direct absorption cross section depends on the angle between the polarization vector $\mathbf{e}$ of the incoming x-ray photon and the directions between the absorbing and neighboring atoms, the XRS cross section depends both on $(\mathbf{e}\cdot\hat{\mathbf{R}}_{\alpha\alpha_1})$ and on $(\mathbf{e}'\cdot\hat{\mathbf{d}}_n)$, i.e., on the orientation of polarization vector $\mathbf{e}'$ of the emission x-ray photon relative to the dipole moment $\mathbf{d}_n$ of an emission transition from an occupied MO $|n\rangle$. This circumstance leads to an untrivial polarization dependence of EXAFS measured in the XRS mode of disordered media like free molecules in the gas phase or noncrystalline solids.

Let us consider the EXAFS of disordered media. In this case the XRS cross sections $\sigma(\omega)$, Eq. (8), and $\sigma^{\mathrm{XA}}(\omega)$, Eq. (11), must be averaged over "molecular" orientations, i.e., over the surroundings close to the absorbing atom. This averaging is equivalent to an averaging over the directions of photon propagations under a fixed angle ζ between the real polarization vectors $\mathbf{e}$ and $\mathbf{e}'$ and is fulfilled by the formula

$$\overline{(e_i'e_j'^{*}e_ke_l^{*})}=\tfrac{1}{6}[\delta_{ij}\delta_{kl}(1-\cos^2\zeta)+\tfrac{1}{5}(\delta_{ij}\delta_{kl}+\delta_{ik}\delta_{jl}+\delta_{il}\delta_{jk})(3\cos^2\zeta-1)]\,. \quad (21)$$

Now the x-ray Raman scattering and x-ray-absorption cross sections, $\sigma(\omega)$ and $\sigma^{\mathrm{XA}}(\omega)$, are described by the same formula, Eq. (11), but with different χ functions (the index "XA" must be removed in the case of XRS). The expression for the EXAFS spectrum measured in XRS mode now becomes

$$\chi=-\mathrm{Im}\sum_{\alpha_1}\frac{e^{2i(kR_{\alpha\alpha_1}+\delta_1^{\alpha})}}{kR_{\alpha\alpha_1}^2}f_{\alpha_1}(\pi)\eta_{\alpha\alpha_1}(\zeta)\,. \quad (22)$$

The polarization function

$$\eta_{\alpha\alpha_1}(\zeta)=\tfrac{3}{5}[2-\cos^2\zeta+(3\cos^2\zeta-1)\cos^2\varphi_{\alpha\alpha_1}] \quad (23)$$

depends on the angle ζ between polarization vectors $\mathbf{e}$ and $\mathbf{e}'$ and on the angle $\varphi_{\alpha\alpha_1}$ between the transition dipole moment $\mathbf{d}_n$ of emission and the direction $\mathbf{R}_{\alpha\alpha_1}$ to atom α_1. To emphasize the difference between ordinary EXAFS measured in the transmission mode and EXAFS measured in the XRS mode we remind the reader that the formula by Sayers, Lytle, and Stern[2,3] for ordinary EXAFS of disordered systems is defined by Eq. (22) with $\eta_{\alpha\alpha_1}(\zeta)=1$. Formula (23) can easily be generalized to nonresonant scattering of light in which $\omega'\neq\omega_{n(\nu)}$ or to the case of strongly overlapping x-ray-emission lines. In the region of resonance fluorescence for arbitrary frequencies ω' of emission photons one can see from the Kramers-Heisenberg formulas (2) and (4) that we need to use in Eq. (23) only a more general definition for the angle $\varphi_{\alpha\alpha_1}$, namely,

$$\cos^2\varphi_{\alpha\alpha_1}=\frac{\sum_n\cos^2\varphi_{\alpha\alpha_1}^{(n)}\Delta(\omega'-\omega_n,\Gamma_n)}{\sum_n d_n^2\Delta(\omega'-\omega_n,\Gamma_n)}\,, \quad (24)$$

where the subscript ν is omitted for the emission resonant frequency $\omega_n=\omega_{n(\nu)}$, because in the EXAFS region the above-mentioned screening effect is negligibly small. The bond angle

$$\cos\varphi_{\alpha\alpha'}^{(n)}=(\hat{\mathbf{d}}_n\cdot\hat{\mathbf{R}}_{\alpha\alpha'}) \quad (25)$$

is the angle between the transition dipole moment $\mathbf{d}_n$ of x-ray emission and the bond direction $\mathbf{R}_{\alpha\alpha'}$. The measurement of these angles solves completely the problem of definition of bond angles. Unfortunately the bond angles $\varphi_{\alpha\alpha'}^{(n)}$ (25) can probably not be measured directly. In accordance with Eqs. (22) and (23) only the angles $\varphi_{\alpha\alpha_1}$ are measurable quantities. The x-ray-emission spectrum often has one or several resonances which do not overlap or only slightly overlap one another. In this case the angles $\varphi_{\alpha\alpha_1}^{(n)}$ and $\varphi_{\alpha\alpha_1}$ coincide if the emission photon frequency ω' is tuned into exact resonance with one of these nonoverlapping resonances $n\rightarrow c$ $(\omega'=\omega_n)$.

IV. OXYGEN EXAFS XRS SPECTRA IN AMORPHOUS SILICON OXIDE

Let us demonstrate the distinct possibilities for structure determination with EXAFS measured in the XRS mode by making some sample calculations on amorphous silicon oxide (a-SiO_2). As shown by contemporary experimental and theoretical investigations,[26–28] it is more relevant to consider an amorphous structure for this compound on a short length scale. But even on this scale the notion of an elementary amorphous unit is not well defined, and it is possible to speak only about a probability to find this elementary unit. Galeener[27] was forced to consider regions of increased order in the form of highly regular rings of bonds, connected into the otherwise more disordered network at sites the special nature of which remains unknown. The structure of n-fold rings and their distribution in vitreous SiO_2 was recently investigated us-

ing molecular-dynamics (MD) calculations.[28] It was found that the sixfold rings were the most abundant ones and that the ring distribution was nearly symmetric around $n=6$. The real ring distribution is quite smooth near $n=6$.[28] Both experiment[26] and theory[28] establish that the rings are not strictly planar. The results of MD calculations for a-SiO_2 compare very well with neutron-diffraction, x-ray-diffraction, and NMR experiments,[28] but not with infrared Raman spectroscopy.[26] The infrared Raman spectra of a-SiO_2 are consistent with the suggestion that this amorphous system contains a substantial concentration of nearly planar threefold rings. Nevertheless, we restrict our attention here to the sixfold planar rings [one of Galeener's models,[27] Fig. 1(a)] only with the purpose to underline more clearly the main idea of the method suggested here.

The sixfold planar ring can be visualized with the help of Fig. 1. This ring is connected to the rest of the network by twelve Si-O bonds. It will be supposed here for simplicity that the outward pairs of oxygen atoms in Fig. 1 are lying in planes perpendicular to the ring plane. The intersection of these planes is a bisector of angle ϕ (O-Si-O angle). We shall use the following calculated values for the Si-O bond length (R), O-Si-O (ϕ), and Si-O-Si (Θ) bond angles: 1.62 Å, 109.5°, 190.5°, respectively.[28] Let us consider the oxygen K-edge EXAFS spectrum. As one can see from Fig. 1(a) the nearest neighbors for each oxygen atom lying in the ring plane are two silicon atoms. The EXAFS method allows one to select signals from different coordinate spheres;[1-4] therefore we shall analyze here the EXAFS signals only of the first and second coordinate spheres caused by the Si_2-O-Si_3 and Si_1-O-Si_4 fragments, respectively (Fig. 1). We shall see below that the x-ray-emission spectrum of the chosen model system

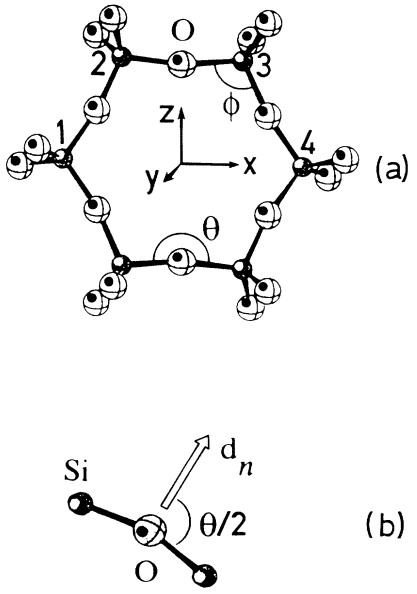

FIG. 1. Planar sixfold ring of silicon oxide. Small and large spheres represent Si and O atoms, respectively. $\phi=109.5°$ and $\Theta=190.5°$ denote O-Si-O and Si-O-Si bond angles.

has several resonances which do not overlap or only slightly overlap with other emission resonances. In this case formula (24) can be simplified to

$$\varphi_{\alpha\alpha'}\simeq\varphi^{(n)}_{\alpha\alpha'}=\cos^{-1}(\hat{\mathbf{d}}_n\cdot\hat{\mathbf{R}}_{\alpha\alpha'}) \tag{26}$$

if the emission photon frequency ω' is tuned into exact resonance with one of these nonoverlapping transitions $n\rightarrow c$. As seen directly from this equation $\varphi_{\alpha\alpha'}=0$ when the dipole moment $\mathbf{d}_n$ of emission transition $n\rightarrow c$ is lying perpendicular to the ring. Let us denote the corresponding value of the χ function (20) as $\chi_\perp$. The angle $\varphi_{\alpha\alpha'}$ is expressed directly through the Si-O-Si bond angle $\Theta(\varphi_{\alpha\alpha'}=\Theta/2)$ if $\mathbf{d}_n$ is the bisector of the Si-O-Si angle lying in the ring plane [Fig. 1(b)]. We mark the χ function (20) in this case as $\chi_\parallel$. As a result we have the following connection between the Si-O-Si bond angle Θ and the experimentally measured values for the χ function:

$$\cos^2\frac{\Theta}{2}=\left[\frac{\chi_\parallel}{\chi_\perp}-1\right]\Xi(\zeta)\ , \tag{27}$$

where the function

$$\Xi(\zeta)=(2-\cos^2\zeta)/(3\cos^2\zeta-1)$$

depends on the polarization vectors $\mathbf{e}$ and $\mathbf{e}'$ through the angle ζ between them (Fig. 2). This formula shows directly how bond angles can be defined by EXAFS measured in the XRS mode. The function $\Xi(\zeta)$ is singular near the angle $\zeta=\cos^{-1}(1/\sqrt{3})$ (Fig. 2). But the relative change of the χ function $(\chi_\parallel/\chi_\perp-1)$ is equal to zero for this angle. Therefore $\cos(\Theta/2)$ defined by Eq. (27) is a regular function. One can see from Eq. (24) that formulas (26) and (27) give only a rough connection between the bond angle $\varphi^{(n)}_{\alpha\alpha'}=\Theta/2$ and the experimentally measured χ function or angle $\varphi_{\alpha\alpha'}$ when the frequency of x-ray emission is tuned into a region of strongly overlapping resonances.

To illustrate the connection between bond angles $\varphi^{(n)}_{\alpha\alpha'}$ and measurable angles $\varphi_{\alpha\alpha'}$ more specifically we have performed *ab initio* calculations of the oxygen x-ray-emission

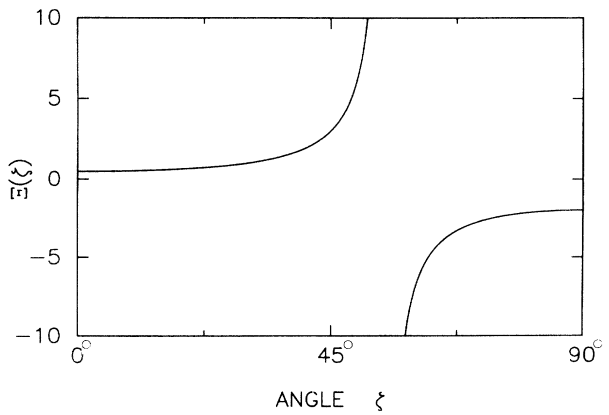

FIG. 2. Dependence of the $\Xi(\zeta)$ function on the angle ζ between polarization vectors $\mathbf{e}$ and $\mathbf{e}'$ of absorption and emission photons [see Eq. (27)].

spectrum of the sixfold ring consisting of 6 silicon and 12 oxygen atoms (see Fig. 1). The O K emission spectrum of the in-plane oxygen was obtained in the frozen-orbital approximation using orbital (Koopmans) energies relative to the ionization threshold and full two-center transition moments. The merits and limitations of this model with respect to more refined and more crude approximation levels have been well investigated for small molecules; see, e.g., Ref. 29. The wave function was expanded in a single ζ basis set employing a broken-symmetry, localized description for the core orbitals. The calculations were carried out with the direct self-consistent-field program DISCO.[30]

Table I collects in C_{2v} symmetry notations the eigenvalues of molecular orbitals, relative values of x-ray-emission intensities, and directions of the dipole moments for the top-site O atom (see Fig. 1). In the C_{2v} point group each symmetry representation is associated with one and only one dipole direction, thereby further simplifying the analysis. A_1 and B_1 are in-plane Σ symmetries, and B_2 and A_2 are out-of-plane Π symmetries, the latter being dipole forbidden. Each pair of out-of-plane oxygen atoms forms the beginning of the next sixfold ring (see Fig. 1), and they are for this reason left out from the present analysis. The spectral distribution of oscillator strengths in the x-ray-emission spectrum and the corresponding symmetry assignments (see Table I and Figs. 3 and 4) give direct connections between bond angles $\varphi_{\alpha\alpha'}^{(n)}$ (25) and spectral features of experimentally measurable angles $\varphi_{\alpha\alpha'}$ (24). The cosine of this angle $\varphi_{\alpha\alpha'}$ was calculated with the help of formula (24) and obtained from the calculations on the sixfold ring (see Table I). Table I shows the existence of four groups (i, k, l, and p) of x-ray-emission resonances of different symmetries with nearly degenerate energies: ($3A_1, 4B_1$), ($4B_2, 5A_1, 5B_1$), ($6A_1, 5B_2$), and ($8B_2, 7A_1$). These nine resonances are presented in Figs. 3 and 4 by only four peaks due to the strong energy degeneracy inside each group. The intensity of each peak i, k, l, and p in Figs. 3 and 4 is equal to the sum of intensities in the corresponding group of resonances.

Let us remember that the eigenvalues of the MO's coincide in the Hartree-Fock approximation with the energies ($\omega_n - I$) of the corresponding x-ray transitions measured relative to the O K ionization threshold I. The oxygen backscattering amplitude $f_O(\pi)$ is small in comparison with the silicon one $f_{Si}(\pi)$.[1,4] Therefore the O K EXAFS signal is defined only by the silicon backscattering. The Fourier transform of the χ function (22) allows one to select the contributions from different coordinate spheres.[1-4] We shall analyze here the contribution from the two first coordinate spheres only. The silicon atoms 2

TABLE I. Computation of the oxygen K x-ray-emission spectrum of sixfold silicon oxide. Energies (eV) are given relative to the ionization threshold. $\cos^2\varphi_{\alpha\alpha'}^{(n)}$ is given for first (1cs) and second (2cs) coordination shells.

No.[a]	MO[b]	Energy	Intensity	1cs $\cos^2\varphi_{\alpha\alpha'}^{(n)}$	2cs $\cos^2\varphi_{\alpha\alpha'}^{(n)}$
(a)	$1B_1(x)$	−21.48	0.97	0.992	0.625
(b)	$2B_1(x)$	−19.47	1.42	0.992	0.625
(c)	$3B_1(x)$	−18.13	0.92	0.992	0.625
(d)	$1A_1(z)$	−16.81	0.73	0.008	0.375
(e)	$1B_2(y)$	−16.16	1.05	0.0	0.0
(f)	$2B_2(y)$	−15.74	2.52	0.0	0.0
(g)	$2A_1(z)$	−14.89	0.91	0.008	0.375
(h)	$3B_2(y)$	−14.70	3.16	0.0	0.0
(i)	$3A_1(z)$	−14.23	1.44	0.008	0.375
(i)	$4B_1(x)$	−14.22	0.51	0.992	0.625
(j)	$4A_1(z)$	−13.92	4.59	0.008	0.375
(k)	$4B_2(y)$	−13.45	4.32	0.0	0.0
(k)	$5A_1(z)$	−13.43	0.68	0.008	0.375
(k)	$5B_1(x)$	−13.42	1.17	0.992	0.625
(l)	$6A_1(z)$	−13.22	7.68	0.008	0.375
(l)	$5B_2(y)$	−13.20	4.30	0.0	0.0
(m)	$6B_1(x)$	−13.08	0.76	0.992	0.625
(n)	$6B_2(y)$	−13.03	2.82	0.0	0.0
(o)	$7B_2(y)$	−12.97	1.29	0.0	0.0
(p)	$8B_2(y)$	−12.47	1.30	0.0	0.0
(p)	$7A_1(z)$	−12.46	5.20	0.008	0.375
(r)	$9B_2(y)$	−12.32	1.37	0.0	0.0
(q)	$8A_1(z)$	−12.22	2.08	0.008	0.375
(s)	$10B_2(y)$	−8.20	1.12	0.0	0.0
(t)	$11B_2(y)$	−7.81	1.92	0.0	0.0
(u)	$12B_2(y)$	−7.68	1.04	0.0	0.0

[a]Labels of resonances of the O K emission spectrum (Figs. 3 and 4).
[b]Direction of the transition dipole moment.

and 3 are lying in the first coordinate sphere, while the silicon atoms 1 and 4 belong to the second coordinate sphere (of atoms in the ring plane, see Fig. 1).

The molecular orbitals of A_1, B_1, and B_2 symmetries and corresponding transition dipole moments $\mathbf{d}_n$ are oriented along the z, x, and y axes, respectively (see Fig. 1 and Table I). The bond angle $\varphi_{\alpha\alpha'}^{(n)}$ for the first coordinate sphere is the one between $\mathbf{d}_n$ and the direction $\mathbf{R}_{O2}$ from oxygen atom O to silicon atom 2 (or 3) [see Fig. 1(a)]. The values of $\cos^2\varphi_{\alpha\alpha'}^{(n)}$ (25) are equal to 0.008, 0.992, and 0 for the emission transitions from MO's of A_1, B_1, and B_2 symmetries, respectively (Table I). The direction $\mathbf{R}_{O1}$ from oxygen atom O to silicon atom 1 (or atom 4) defines the bond angle $\varphi_{\alpha\alpha'}^{(n)}$ for the second coordinate sphere (Fig. 1) and as a result $\cos^2\varphi_{\alpha\alpha'}^{(n)}=0.375$, 0.625, and 0 for MO's of A_1, B_1, and B_2 symmetries, respectively (Table I). Let us consider now how these bond angles $\varphi_{\alpha\alpha'}^{(n)}$ can be found from the experimentally measurable bond angles $\varphi_{\alpha\alpha'}$ (24). We shall use here $\Gamma=0.075$ eV since this seems to be a characteristic lifetime broadening of the O K emission lines of many molecules,[31] and since some modern experimental equipment makes it possible to obtain x-ray-emission spectra with resolution close to the lifetime broadening. Figures 3 and 4 and Table I demonstrate that in this case for the slightly overlapping resonances (a,b,c) and (s,t,u) the experimentally measurable $\cos^2\varphi_{\alpha\alpha'}$ factors are close to the 0.992 (0.625) and 0 (0)

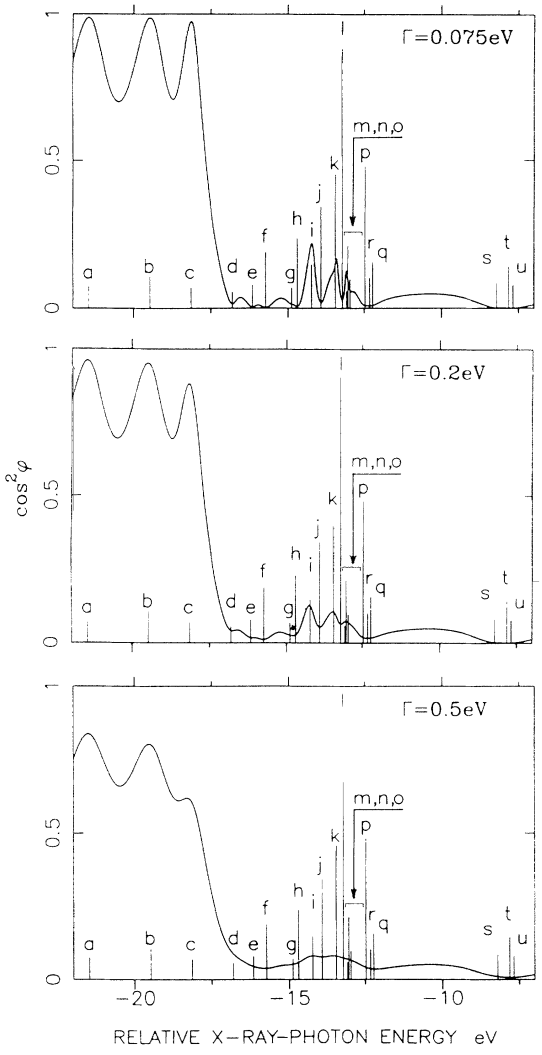

FIG. 3. Dependence of the experimentally measurable bond angle (24) on the energy of an x-ray-emission photon (solid line) and the HWHM ($\Gamma=\Gamma_n$) for the first coordinate sphere. Positions and relative intensities of the ordinary oxygen x-ray-emission spectrum of the planar sixfold ring in amorphous SiO_2 are displayed for comparison by vertical bars. The energy of an x-ray-emission photon is given relative to the O K ionization threshold. The values of $\cos^2\varphi_{\alpha\alpha'}^{(n)}$ for bond angles (25) are 0, 0.008, and 0.992 for the O K emission transitions from MO's of B_2, A_1, and B_1 symmetries, respectively.

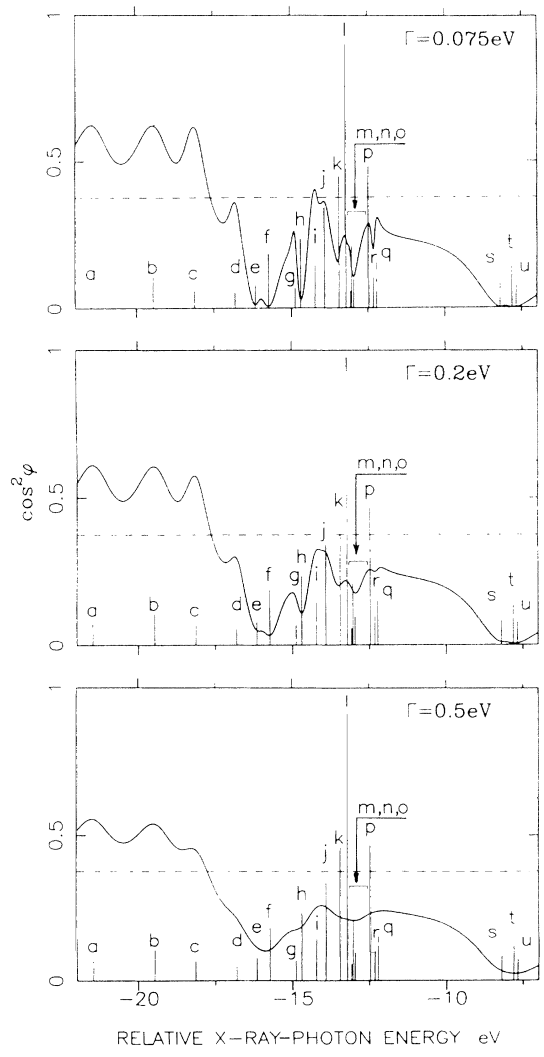

FIG. 4. Dependence of the experimentally measurable bond angle (24) on the energy of an x-ray-emission photon (solid line) and the HWHM ($\Gamma=\Gamma_n$) for the second coordinate sphere. The values 0.375 and 0.625 of $\cos^2\varphi_{\alpha\alpha'}$ for bond angles (25) presented by horizontal lines correspond to emission transitions from MO's of A_1 and B_1 symmetries, respectively. $\cos^2\varphi_{\alpha\alpha'}=0$ for transitions from MO's of B_2 symmetry.

given by the true bond angles $\varphi_{\alpha\alpha'}^{(n)}$. Here the first value corresponds to the first coordinate sphere and the one in parentheses to the second sphere. The same picture is obtained for the resonances (d,e,f) which give values of $\cos^2\varphi_{\alpha\alpha'}$ close to 0.008 (0.375), 0 (0), and 0 (0), respectively. The agreement between $\varphi_{\alpha\alpha'}$ and $\varphi_{\alpha\alpha'}^{(n)}$ is not so good in the region of close-lying resonances $(g-q)$ except for the resonances h and j. The real width of the emission lines is defined by both the lifetime and the instrumental broadenings. We have estimated the role of the latter by simply increasing Γ_n. Figures 3 and 4 show an increased agreement between measurable $(\varphi_{\alpha\alpha'})$ and true $(\varphi_{\alpha\alpha'}^{(n)})$ bond angles when the total width of emission resonance decreases. One should note that the role of emission resonance overlapping (see Figs. 3 and 4) is exaggerated here. The composite Voigt function is closer to a Gaussian $\exp\{-[(\omega'-\omega_n)/\Gamma_n]^2\}$ when the instrumental broadening dominates over the lifetime broadening. But the overlap of Gaussians is smaller than the overlap of the Lorentzian Δ functions (3). As a result the EXAS signal described by $\cos^2\varphi_{\alpha\alpha'}$ (24) depends not so strongly on the instrumental broadening as demonstrated by Figs. 3 and 4.

V. DISCUSSION

A. Experimental feasibility

In this subsection we consider in general terms the possibilities for obtaining signals of EXAFS detected in the XRS mode. Let us remember that the spectral resolution required for x-ray photons in an EXAFS experiment does not need to be very sharp. To detect EXAFS oscillations a resolution element as large as ~ 5 eV can be allowed.[4] The EXAFS experiments with fluorescence-yield detection carried out by Eisebitt *et al.*[5] and Adler *et al.*[6] (see also Refs. 1 and 4) gave good signal-to-noise ratios. Solid-state fluorescence detectors were used in both experiments because the spectral resolution for the corresponding emission can be very low. For example, Eisebitt *et al.*[5] were using a germanium detector that gave a resolution for Co L emission of about 100 eV. On the other hand, structure investigations by the method suggested here require a spectral resolution of the order of the separation of molecular-orbital levels, ~ 1 eV (see Figs. 3 and 4 and Table I). Because the FY signal decreases when narrow emission lines are recorded instead of the total fluorescence yield, the signal-to-noise ratio becomes more crucial. In the presentation given above thin samples were implicitly assumed. A general expression for the fluorescence signal of a sample with arbitrary thickness can be obtained following the method outlined by Stöhr[1] and Lee *et al.*[4] The latter authors[4] predict the EXAFS signal-to-noise ratio for 1 sec of integration in the small-thickness limit to be

$$\frac{S}{N}=[I_{\text{inc}}\epsilon(\Omega/4\pi)\mu X]^{1/2}\frac{\Delta\mu}{\mu}\ , \tag{28}$$

where I_{inc} is the incoming photon flux, ϵ is the fluorescence yield, $\Omega/4\pi$ is the solid angle acceptance of fluorescence, X is the sample thickness, and $\Delta\mu$ is the EXAFS modulation of the absorption coefficient μ. For the feasibility of EXAFS XRS it is relevant to note that current storage rings have x-ray photon fluxes as large as $I_{\text{inc}}\sim 10^{14}-10^{15}$ photons/sec.[32] We need to estimate the fluorescence yield ϵ for a single line of x-ray-emission valence bands. This can simply be achieved by dividing the total FY for a low-Z atom[4] ($\sim 10^{-3}$) by the number of valence MO's, which for ordinary molecules is in the range of 10–100. A reliable estimation of a single-line FY is thus $\epsilon\sim 10^{-5}$. The suggested values $\Omega/4\pi\sim 10^{-4}$, $\Delta\mu/\mu\sim 10^{-2}$, and $\mu X\sim 1$ lead to the following estimation of the signal-to-noise ratio: ~ 10 in 1 sec. Although not strong this ratio allows some optimism for realistic measurements of bond angles by the method suggested here. For instance, going to $Z=20$ (calcium), the fluorescence yield is raised to $\sim 10^{-1}$, thereby raising the signal-to-noise ratio by one order of magnitude.

We have not considered the vibronic structure of x-ray-emission bands. However, vibronic excitations do not change the polarization function $\eta_{\alpha\alpha_1}(\zeta)$, but lead only to an additional broadening of the fluorescence resonance of the order of ~ 1 eV (including lifetime-vibrational interference contributions specific for the XRS process[8,9]). This follows from the general rule that only totally symmetric vibrational modes are excited with significant intensity in electronic absorption and emission. Strong vibronic coupling between close-lying states of different symmetries can of course change the analysis. In the case of amorphous systems other, and maybe more important, mechanisms for broadening of emission lines exist. Referring to the example discussed in Sec. IV the concentration of sixfold rings with respect to other structures must be sufficiently large. (As shown in Ref. 28 the abundance of sixfold rings is only 1.5 and 1.8 times larger than of five- and sevenfold rings, respectively.) Different structures (here rings) have different characteristic x-ray-emission spectra, and unless they can be separated, e.g., by identifying specific chemical shifts, an analysis of the kind presented in Sec. IV may become difficult.

B. EXAFS measured in the nonradiative scattering mode

EXAFS can be detected in several ways, either directly in the transmission mode, or indirectly by measuring the products of absorption, namely, the fluorescent radiation or the nonradiative Auger or secondary electrons.[1,4] The case of fluorescence photons (or XRS) detection was thus investigated in the previous sections. Let us now consider shortly the detection of the nonradiative, secondary electrons for measuring EXAFS. The cross section of this process is considerably larger than that of XRS for low-Z atoms. Therefore the Auger process has certain advantages in comparison with x-ray Raman scattering.[1,4] To make an analogy with XRS we consider the following Auger process. An incoming x-ray photon excites a core electron into the continuum state ψ_k, and is followed by an electron decay from MO ψ_n to core shell c. The energy of this transition is transferred through a Coulomb interelectron interaction

$$(\mathbf{p}n|cn)=\int \psi_{\mathbf{p}}^{*}(\mathbf{r}_1)\psi_n(\mathbf{r}_1)\frac{1}{r_{12}}\psi_c^{*}(\mathbf{r}_2)\psi_n(\mathbf{r}_2)d\mathbf{r}_1 d\mathbf{r}_2 \tag{29}$$

to the second electron from this MO. Here we have for simplicity considered an Auger transition that empties two electrons from the same orbital, for which the exchange term is lacking. $\psi_{\mathbf{p}}$ denotes the continuum orbital housing the expelled electron. The amplitude of this process,

$$\alpha^{1/2}\frac{(\mathbf{e}^{*}\cdot\mathbf{d}_{\mathbf{k}})(\mathbf{p}_n|cn)}{\omega-\omega_{\mathbf{k}}+i\Gamma_{\mathbf{k}}}\ , \tag{30}$$

strongly reminds one of the XRS amplitude (4). The cross section of this process is proportional to (2), where the Δ function must be replaced by $\Delta(\omega-E_{\mathbf{p}}-E_{\mathbf{k}}+2E_n,\Gamma')$ in accordance with the energy conservation law,[10] Γ' denoting here the lifetime broadening of the final state. The cross section (2) after integration over $\mathbf{k}$ will depend on the mutual orientations of vectors $\mathbf{e}$, $\mathbf{p}$, and $\mathbf{R}_{\alpha\alpha'}$ and on the space orientation of MO ψ_n. The orientation of this MO in the case of a K spectrum is defined only by the direction of the transition dipole moment $\mathbf{d}_n$. It is then easy to understand that the cross section (2) for the nonradiative process (30) for disordered systems only depends on the scalar products $(\mathbf{e}\cdot\mathbf{p})$ and $(\mathbf{d}_n\cdot\mathbf{R}_{\alpha\alpha'})$. As a result also EXAFS detected in the nonradiative Auger mode will be described by the χ function (22), but with a different polarization function $\eta_{\alpha\alpha'}(\xi)$ depending on the angles $\xi=\cos^{-1}(\hat{\mathbf{e}}\cdot\hat{\mathbf{p}})$ and $\varphi_{\alpha\alpha'}$. The spectral dependence of the experimentally measurable bond angle $\varphi_{\alpha\alpha'}$ on the energy $E_{\mathbf{p}}$ of the Auger electron reminds one of those shown in Figs. 3 and 4 and makes it possible to determine bond angles just as when EXAFS is detected in the XRS mode. Of course, the theory sketched in this section is far from complete. In a more general theory the Coulomb integral in Eq. (30) must be replaced by the corresponding T matrix, which takes into account interelectron correlation effects and postcollisional effects.[33] A more detailed account of EXAFS Auger spectroscopy will be presented in a forthcoming paper.[34]

VI. CONCLUSION

In this work we have presented a theory for extended x-ray-absorption fine structure measured in the x-ray Raman-scattering mode. We have shown the dependence of EXAFS detected in the XRS mode on the scalar product of a transition dipole moment of emission and the direction of an internuclear axis. From this factor one can obtain directional and comformational information in the "molecular frame." By choosing a specific resonance frequency one determines a specific orientation for the transition dipole in this frame, which allows an inspection "within" the molecule of bond directions with respect to the chosen transition dipole direction. EXAFS detected in the XRS mode can even be used for measurements of bond angles of disordered systems like amorphous glasses or free molecules, and will be applicable for structure investigations of liquids, molecular layers on surfaces, and surface melting.

ACKNOWLEDGMENTS

We are grateful to J. Nordgren and N. Wassdahl for helpful discussions. This work was supported by grants from the University of Uppsala (F.Kh.G) and from Cray Research Inc. (H. Å.).

APPENDIX: THE GREEN'S FUNCTION IN THE MUFFIN-TIN POTENTIAL

The muffin-tin approximation of a real potential experienced by the photoelectron leads to the following expansions of the Green's function over spherical functions $Y_{lm}(\hat{\boldsymbol{\rho}})$ inside of the αth MT sphere ($\rho,\rho'\le a_\alpha$) with a radius a_α:

$$G_E^{+}(\mathbf{r},\mathbf{r}')=k\sum_L R_L^{\alpha}(\boldsymbol{\rho}_<)N_L^{\alpha *}(\boldsymbol{\rho}_>) + k\sum_{LL'}[e^{i\delta_l^{\alpha}}G_{LL'}^{\alpha\alpha}e^{i\delta_{l'}{}^{\alpha}}-i\delta_{LL'}]R_L^{\alpha}(\boldsymbol{\rho})R_{L'}^{\alpha *}(\boldsymbol{\rho}') \tag{A1}$$

and inside the αth and α'th MT spheres ($\rho\le a_\alpha$, $\rho'\le a_{\alpha'}$):

$$G_E^{+}(\mathbf{r},\mathbf{r}')=k\sum_{LL'}e^{i\delta_l^{\alpha}}G_{LL'}^{\alpha\alpha'}e^{i\delta_{l'}^{\alpha'}}R_L^{\alpha}(\boldsymbol{\rho})R_{L'}^{\alpha' *}(\boldsymbol{\rho}')\ , \tag{A2}$$

where $L=(l,m)$, $k=(2E)^{1/2}$,

$$R_L^{\alpha}(\boldsymbol{\rho})=R_l^{\alpha}(\rho)Y_{lm}(\hat{\boldsymbol{\rho}})\ ,\quad N_L^{\alpha}(\boldsymbol{\rho})=N_l^{\alpha}Y_{lm}(\hat{\boldsymbol{\rho}})\ , \tag{A3}$$

$R_l^{\alpha}(\rho)$ and $N_l^{\alpha}(\rho)$ are the regular and singular lth radial-wave solutions in the potential $V_\alpha(\rho)$ of the αth muffin tin; δ_l^{α} is the scattering phase of the lth partial wave at the αth atom, $\mathbf{r}=\mathbf{R}_\alpha+\boldsymbol{\rho}$, $\rho_>=\max(\rho,\rho')$, and $\rho_<=\min(\rho,\rho')$. The full Green's function $G_{LL'}^{\alpha\alpha'}$ defined relative to two scattering centers at $\mathbf{R}_\alpha$ and $\mathbf{R}_{\alpha'}$ satisfies the equation

$$G_{LL'}^{\alpha\alpha'}=g_{LL'}^{\alpha\alpha'}+\sum_{\alpha''L''}g_{LL''}^{\alpha\alpha''}t_{l''}^{\alpha''}G_{L''L'}^{\alpha''\alpha'}\ . \tag{A4}$$

The diagonal t matrix element $t_l^{\alpha}(E)$ is related to the phase shift $\delta_l^{\alpha}(E)$ by

$$t_l^{\alpha}=-\sin(\delta_l^{\alpha})e^{i\delta_l^{\alpha}}\ . \tag{A5}$$

The matrix elements of the free-electron Green's function $g(\mathbf{r},\mathbf{r}')$

$$g_{LL'}^{\alpha\alpha'}=-(1-\delta_{\alpha\alpha'})4\pi\sum_{l''}i^{l+l''-l'+1}C_{LL'L''}H_{L''}(\mathbf{R}_{\alpha\alpha'}) \tag{A6}$$

are expressed through the Gaunt coefficients

$$C_{LL'L''}=\int d\hat{\mathbf{k}}\ Y_L^{*}(\hat{\mathbf{k}})Y_{L'}(\hat{\mathbf{k}})Y_{L''}(\hat{\mathbf{k}}) \tag{A7}$$

and the spherical wave

$$H_L(\mathbf{R})=h_l^{+}(kR)Y_{lm}(\hat{\mathbf{R}})\ , \tag{A8}$$

where $h_l^{+}(x)$ is the spherical Hankel function, and $\mathbf{R}_{\alpha\alpha'}=\mathbf{R}_\alpha-\mathbf{R}_{\alpha'}$.

*Permanent address: Institute of Automation and Electrometry, 630090 Novosibirsk, Russia.

[1]J. Stöhr, *NEXAFS Spectroscopy* (Springer-Verlag, Berlin, 1992).
[2]D. E. Sayers, F. W. Lytle, and E. A. Stern, *Advances in X-ray Analysis* (Plenum, New York, 1970), Vol. 13, p. 248.
[3]D. E. Sayers, F. W. Lytle, and E. A. Stern, J. Non-Cryst. Solids **8-10**, 401 (1972).
[4]P. A. Lee, P. H. Citrin, P. Eisenberger, and B. M. Kincaid, Rev. Mod. Phys. **53**, 769 (1981).
[5]S. Eisebitt, J.-E. Rubensson, T. Böske, and W. Eberhardt, Phys. Rev. B **48**, 17 388 (1993).
[6]D. L. Adler, I. R. Collins, X. Liang, S. J. Murray, G. S. Leatherman, K.-D. Tsuei, E. E. Chaban, S. Chandavarkar, R. McGrath, R. D. Diehl, and P. H. Citrin, Phys. Rev. B **48**, 17 445 (1993).
[7]F. Kh. Gel'mukhanov, L. N. Mazalov, and A. N. Shklyaeva, Zh. Eksp. Teor. Fiz. **69**, 1971 (1975) [Sov. Phys. JETP **42**, 1001 (1975)].
[8]F. Kh. Gel'mukhanov, L. N. Mazalov, and A. V. Kondratenko, Chem. Phys. Lett. **46**, 133 (1977).
[9]A. Cesar, H. Ågren, and V. Carravetta, Phys. Rev. A **40**, 187 (1989).
[10]T. Åberg and B. Crasemann, in *X-ray Resonant (Anomalous) Scattering*, edited by K. Fisher, G. Materlik, and C. Sparks (Elsevier, Amsterdam, in press).
[11]F. Kh. Gel'mukhanov and H. Ågren, Phys. Lett. A **185**, 407 (1995).
[12]The orientation of the adsorbed molecule relative to a surface can be determined using the NEXAFS method (Ref. 1).
[13]F. Kh. Gel'mukhanov and L. N. Mazalov, Opt. Spectrosc. **42**, 371 (1977).
[14]R. Mayer, D. W. Lindle, S. H. Southworth, and P. L. Cowan, Phys. Rev. A **43**, 235 (1991).
[15]J. J. Sakurai, *Advanced Quantum Mechanics* (Addison-Wesley, Reading, MA, 1967), Chap. 2.
[16]L. Fonda, J. Phys. Condens. Matter **4**, 8269 (1992).
[17]C. A. Ashley and S. Doniach, Phys. Rev. B **11**, 1279 (1975).
[18]R. V. Vedrinskii and A. A. Novakovich, Fiz. Metal. Metalloved. **39**, 7 (1975).
[19]L. N. Mazalov, F. Kh. Gel'mukhanov, and V. M. Chermoshentsev, J. Struct. Chem. (USSR) **15**, 975 (1975).
[20]J. J. Rehr and E. Stern, Phys. Rev. B **14**, 4413 (1976).
[21]V. M. Chermoshentsev, L. N. Mazalov, and F. Kh. Gel'mukhanov, J. Struct. Chem. (USSR) **20**, 175 (1979).
[22]P. A. Lee and J. B. Pendry, Phys. Rev. B **11**, 2795 (1975).
[23]W. L. Schaich, Phys. Rev. B **14**, 4420 (1976).
[24]J. J. Rehr and R. C. Albers, Phys. Rev. B **41**, 8139 (1990).
[25]J. J. Rehr, R. C. Albers, and S. I. Zabinsky, Phys. Rev. Lett. **69**, 3397 (1992).
[26]R. A. Barrio, F. L. Galeener, E. Matínez, and R. J. Elliott, Phys. Rev. B **48**, 15 672 (1993).
[27]F. L. Galeener, J. Non-Cryst. Solids **49**, 53 (1982).
[28]J. P. Rino, I. Ebbsjö, R. K. Kalia, A. Nakano, and P. Vashishta, Phys. Rev. B **47**, 3053 (1993).
[29]H. Ågren and A. Flores-Riveros, J. Electron Spectrosc. **56**, 259 (1991).
[30]J. Almlöf, K. Faegri, Jr., and K. Korsell, J. Comput. Chem. **3**, 385 (1982).
[31]P. Glans, J. Nordgren, H. Ågren, and A. Cesar, J. Phys. B **98**, 6417 (1993).
[32]Lawrence Berkeley Laboratory Report No. PUB-643, Rev. 2, 1989 (unpublished).
[33]F. Gel'mukhanov and H. Ågren (unpublished).
[34]T. Åberg and J. Tulkki, in *Atomic Inner Shell Physics*, edited by B. Crasemann (Plenum, New York, 1985).

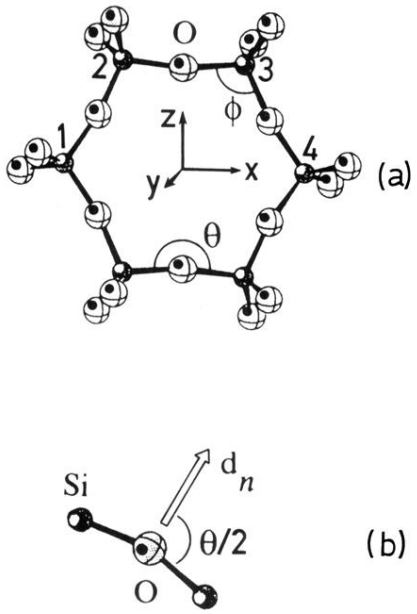

FIG. 1. Planar sixfold ring of silicon oxide. Small and large spheres represent Si and O atoms, respectively. $\phi = 109.5°$ and $\Theta = 190.5°$ denote O-Si-O and Si-O-Si bond angles.